

# Scale-dependent bias due to primordial vector field

Maresuke Shiraishi<sup>1\*</sup>, Shuichiro Yokoyama<sup>2</sup>, Kiyotomo Ichiki<sup>1,3</sup>  
and Takahiko Matsubara<sup>1,3</sup>

<sup>1</sup>*Department of Physics and Astrophysics, Nagoya University, Nagoya, Aichi, 464-8602, Japan*

<sup>2</sup>*Institute for Cosmic Ray Research, University of Tokyo, 5-1-5 Kashiwa-no-Ha, Kashiwa, Chiba, 277-8582, Japan*

<sup>3</sup>*Kobayashi-Maskawa Institute for the Origin of Particles and the Universe, Nagoya University, Nagoya, Aichi, 464-8602, Japan*

## ABSTRACT

Anisotropic stress due to primordial Gaussian vector fields creates the non-Gaussianity in curvature perturbation. We newly provide a generation mechanism of the scale-dependent bias induced by such a non-Gaussian source. We find a simple relation between the amplitude of the non-Gaussianity from the vector field and the local-type nonlinearity parameter, and demonstrate its consistency at large scales and tiny deviation at small scales in the scale-dependent bias for several spectral indices of the vector field and redshifts. By interpreting the vector field as the primordial large scale magnetic field, we show that the magnetic field certainly realizes the negative scale-dependent bias. The scale-dependent bias will become a new window on the primordial vector field.

**Key words:** scale-dependent bias – non-Gaussianity – vector field

## 1 INTRODUCTION

The cosmological models with vector fields have been considered in order to explain several observational consequences of large-scale cosmic magnetic fields and the statistical anisotropy of the Universe (e.g., Widrow (2002); Bamba & Sasaki (2007); Martin & Yokoyama (2008); Watanabe et al. (2010)). Although there has yet to be a successful model of inflationary magnetogenesis as shown in Bamba & Yokoyama (2004); Kanno et al. (2009); Demozzi et al. (2009); Demozzi & Ringeval (2012); Suyama & Yokoyama (2012); Fujita & Mukohyama (2012), such a vector field provides interesting imprints on the cosmic microwave background (CMB) and gravitational waves (e.g., Ackerman et al. (2007); Watanabe et al. (2011); Sorbo (2011); Barnaby et al. (2012)). Nowadays, beyond the framework of magnetogenesis, the global analyses involving the higher-order cosmological perturbation have attracted attention.

The non-Gaussianity of primordial fluctuations is a powerful observable in order to extract true answers from a huge number of the models for the early Universe; therefore there are a lot of approaches from both theoretical and observational sides (for review, see e.g., Bartolo et al. (2004); Komatsu (2010)). One can see beneficial bounds on the amplitude and the spectral tilt of the non-Gaussianity, which depend on theoretical parameters associated with the scalar perturbation, from

the higher-order correlations of CMB fluctuations (e.g., Sefusatti et al. (2009); Komatsu et al. (2011); Smidt et al. (2010); Hikage & Matsubara (2012); Becker & Huterer (2012); Becker et al. (2012)). On the other hand, one can also find studies which evaluate the non-Gaussian impacts of not only pure scalar perturbation but also the vector perturbation in the context of the phenomenology of the primordial vector or electromagnetic field (e.g., Brown & Crittenden (2005); Yokoyama & Soda (2008); Karciauskas et al. (2009); Valenzuela-Toledo & Rodriguez (2010); Dimastrogiovanni et al. (2010); Barnaby & Peloso (2011); Barnaby et al. (2011, 2012); Caldwell et al. (2011); Motta & Caldwell (2012); Jain & Sloth (2012); Bartolo et al. (2012)). These non-trivial non-Gaussianities have been investigated using the CMB power spectra and bispectra (Shiraishi et al. (2012); Shiraishi (2012); Shiraishi et al. (2012)).

Together with the CMB spectra, the scale-dependent bias, which is defined in the difference between the density field of biased object and the matter density field, is a good estimator of the primordial non-Gaussianity of curvature perturbation (see e.g., Slosar et al. (2008); Verde (2010)). Recently, to explore the scale dependence of the primordial bispectrum via the shape of the bias parameter is gaining a lot of attention. While the bias parameter generated from the exact local-type non-Gaussianity has  $k^{-2}$  dependence, there are models which predict the deviation from it (e.g., Shandera et al. (2011)). The bispectrum shape of curvature perturbation sourced from the vector field directly reflects the tilt of the power spectrum of vector fields, which de-

\* E-mail: mare@nagoya-u.jp

pends strongly on the generation mechanism of the vector field. In this sense, the shape of the bias parameter is expected to afford a useful clue to the nature of the primeval vector field.

This paper newly focuses on the impacts of the non-Gaussianity induced by the vector field on the scale-dependent bias. To estimate this, we assume the existence of the Gaussian vector field in the early Universe. Accordingly, the anisotropic stress arising from the square of this field obeys the chi-square statistics and creates non-Gaussian curvature perturbation. In this paper, we adapt this curvature perturbation as a source of the scale-dependent bias. By the analysis of the bispectrum shape, we find that such a non-Gaussianity has the local-type configuration and hence we derive a relation between the amplitudes and the spectral indices of the local-type non-Gaussianity and those of the vector field. By applying a general formalism for the scale-dependent bias induced by the primordial bispectrum, which is based on the integrated perturbation theory (iPT) (Matsubara (2011)) and has been recently reported in Matsubara (2012), we compute the bias parameter from the vector field and confirm the validity of the above relation even in the scale-dependent bias. At the same time, we observe tiny deviation from the local-type bias at small scales. We also analyze the wavenumber and redshift dependences of the scale-dependent bias. The primordial magnetic field is a candidate of this vector field. Applying formulae for the vector field, we reach an interesting fact that the scale-dependent bias from the magnetic field has negative values.

This paper is organized as follows. In the next section, we present a generation mechanism of the non-Gaussian curvature perturbation induced by the primordial vector field. In Section 3, we compute the scale-dependent bias originated from such a non-Gaussianity for several spectral indices of the vector field and redshifts. The final section is devoted to the summary and discussion of this paper.

## 2 PRIMORDIAL NON-GAUSSIANITY GENERATED FROM VECTOR FIELD

In this section, we firstly give a discussion on the non-Gaussian curvature perturbation, which is generated from anisotropic stress induced by some sort of vector field in the early Universe. Next, we show that the electromagnetic field, which may occur in inflation, can produce such non-Gaussian anisotropic stress.

### 2.1 Curvature perturbation induced by anisotropic stress

If anisotropic stress, which scales like radiations ( $\propto a^{-4}$  with  $a$  being the scale factor normalized by the present epoch), occurs deep in the radiation-dominated era, it acts as a source term of the Einstein equation. Then, the curvature perturbation experiences the logarithmic growth even on superhorizon scales. However, such anisotropic stress is compensated by the neutrino anisotropic stress posterior to neutrino decoupling and therefore the enhancement of the curvature perturbation stops. The resultant comoving curvature perturbation on superhorizon scales is evaluated as

(Kojima et al. (2010); Shaw & Lewis (2010))

$$\mathcal{R}_V(\mathbf{k}) \approx R_\gamma \ln \left( \frac{\tau_\nu}{\tau_V} \right) \frac{3}{2} Q_i^j(\hat{\mathbf{k}}) \Pi_{Vj}^i(\mathbf{k}), \quad (1)$$

where  $\tau_\nu$  and  $\tau_V$  is the conformal time of neutrino decoupling and the generation of anisotropic stress,  $R_\gamma \approx 0.6$  is the ratio of the energy density between photons and all relativistic particles,  $Q_i^j(\hat{\mathbf{k}}) \equiv -\hat{k}^j \hat{k}_i + \frac{1}{3} \delta_i^j$ , and  $\hat{\cdot}$  denotes a unit vector<sup>1</sup>. Anisotropic stress normalized by photon's energy density,  $\Pi_{Vj}^i$ , is defined as the traceless part of the energy momentum tensor:

$$T_{Vj}^i(\mathbf{k}, \tau) \equiv \frac{\rho_{\gamma,0}}{a^4} \left[ \Delta_V(\mathbf{k}) \delta_j^i + \Pi_{Vj}^i(\mathbf{k}) \right], \quad (2)$$

with  $\rho_{\gamma,0}$  and  $\Delta_V$  being the present photon's energy density and the isotropic stress, respectively. The solution (1) is corresponding to the so-called passive mode in the context of the magnetized cosmology (Shaw & Lewis (2010)).

Equation (1) indicates that the statistical property of  $\mathcal{R}_V$  directly reflects that of  $\Pi_{Vj}^i$ . Thus, if  $\Pi_{Vj}^i$  consists of the square of the Gaussian vector field as  $\Pi_{Vj}^i(\mathbf{x}) = f_V V^i(\mathbf{x}) V_j(\mathbf{x})$ , whose Fourier components are

$$\Pi_{Vj}^i(\mathbf{k}) = f_V \int \frac{d^3 \mathbf{k}'}{(2\pi)^3} V^i(\mathbf{k}') V_j(\mathbf{k} - \mathbf{k}'), \quad (3)$$

$\mathcal{R}_V$  obeys the non-Gaussian statistics and finite higher-order correlation functions can be produced. Here, a dimensionless coefficient,  $f_V$ , behaves like the non-linearity parameter of the local-type non-Gaussianity (Komatsu & Spergel (2001)). In Section 2.3, by considering the electromagnetic action in absence of the conformal invariance, we will see that  $f_V$  corresponds to its coupling.

### 2.2 Bispectrum of curvature perturbations

Once the power spectrum of  $V_i$  is given by

$$\langle V^i(\mathbf{k}) V_j(\mathbf{k}') \rangle = (2\pi)^3 \frac{P_V(k)}{2} P_j^i(\hat{\mathbf{k}}) \delta(\mathbf{k} + \mathbf{k}'), \quad (4)$$

with  $P_V(k) \equiv \frac{2\pi^2}{k^3} A_V \left( \frac{k}{k_*} \right)^{n_V-1}$  and  $P_j^i(\hat{\mathbf{k}}) \equiv \delta_j^i - \hat{k}^i \hat{k}_j$ , the bispectrum of  $\mathcal{R}_V$  is expressed as

$$\begin{aligned} & \left\langle \prod_{n=1}^3 \mathcal{R}_V(\mathbf{k}_n) \right\rangle \\ &= \left[ \prod_{n=1}^3 R_\gamma \ln \left( \frac{\tau_\nu}{\tau_V} \right) \frac{3}{2} Q_{i_n}^{j_n}(\hat{\mathbf{k}}_n) f_V \int d^3 \mathbf{k}'_n P_V(k'_n) \right] \\ & \quad \times \delta(\mathbf{k}_1 - \mathbf{k}'_1 + \mathbf{k}_3) \delta(\mathbf{k}_2 - \mathbf{k}'_2 + \mathbf{k}'_1) \delta(\mathbf{k}_3 - \mathbf{k}'_3 + \mathbf{k}'_2) \\ & \quad \times P_{j_2}^{i_1}(\hat{\mathbf{k}}_1) P_{j_1}^{i_3}(\hat{\mathbf{k}}_3) P_{j_3}^{i_2}(\hat{\mathbf{k}}_2). \end{aligned} \quad (5)$$

As one can see, this involves an additional convolution due to the six-point function of the Gaussian vector fields. To obtain the actual bispectrum, we need to overcome this complicated convolution by a skillful manner. For a case that the power spectrum is nearly scale-invariant as  $n_V \sim 1$ , the contributions of three poles at  $k'_1, k'_2, k'_3 \sim 0$  in the integrand dominate over those in equation (5). By picking

<sup>1</sup> On the comoving gauge,  $\mathcal{R}$  is related to the scalar metric perturbation as  $g_{ij} = a^2 e^{2\mathcal{R}} \delta_{ij}$ .

up only these pole contributions in the same manner as Shiraishi et al. (2012):

$$\begin{aligned} & \int d^3\mathbf{k}' P_V(k') P_j^i(\hat{\mathbf{k}}') \\ & \rightarrow \beta_{n_V} \int_0^{k_*} k'^2 dk' P_V(k') \int d^2\hat{\mathbf{k}}' P_j^i(\hat{\mathbf{k}}') \\ & = 2\pi^2 A_V \frac{\beta_{n_V}}{n_V - 1} \frac{8\pi}{3} \delta_j^i \quad (n_V > 1), \end{aligned} \quad (6)$$

and dealing with contractions, we obtain the reduced formula for  $n_V \sim 1 (> 1)$  as

$$\left\langle \prod_{n=1}^3 \mathcal{R}_V(\mathbf{k}_n) \right\rangle \equiv (2\pi)^3 B_{\mathcal{R}_V}(k_1, k_2, k_3) \delta\left(\sum_{n=1}^3 \mathbf{k}_n\right), \quad (7)$$

where

$$B_{\mathcal{R}_V} \approx \left[ \frac{3}{2} \pi F_V \right]^3 \frac{\beta_{n_V}}{n_V - 1} k_*^{2(1-n_V)} \frac{8\pi}{3} S_V(k_1, k_2, k_3), \quad (8)$$

$$F_V \equiv f_V A_V R_\gamma \ln\left(\frac{\tau_V}{\tau_V}\right). \quad (9)$$

Here, we introduce  $k_* = 0.002 \text{Mpc}^{-1}$  and  $\beta_{n_V}$  as a normalization scale used in the WMAP analysis (Komatsu et al. (2011)) and a factor which should be determined by the comparison with the exact bispectrum, respectively. From numerical studies, we obtain some specific values as  $\beta_{1.1} = 0.785$  and  $\beta_{1.01} = 1.036$ <sup>2</sup>.

The shape function of the bispectrum is given by

$$\begin{aligned} S_V &= \left[ \prod_{n=1}^3 Q_{i_n}^{j_n}(\hat{\mathbf{k}}_n) \right] \\ & \times \left[ k_1^{n_V-4} k_2^{n_V-4} \delta_{j_2}^{i_1} P_{j_1}^{i_3}(\hat{\mathbf{k}}_1) P_{j_3}^{i_2}(\hat{\mathbf{k}}_2) \right. \\ & \quad + k_2^{n_V-4} k_3^{n_V-4} P_{j_2}^{i_1}(\hat{\mathbf{k}}_2) P_{j_1}^{i_3}(\hat{\mathbf{k}}_3) \delta_{j_3}^{i_2} \\ & \quad \left. + k_1^{n_V-4} k_3^{n_V-4} P_{j_2}^{i_1}(\hat{\mathbf{k}}_1) \delta_{j_3}^{i_2} P_{j_3}^{i_2}(\hat{\mathbf{k}}_3) \right] \\ & = \frac{1}{36} \left[ k_1^{n_V-4} k_2^{n_V-4} + 2 \text{ perms.} \right] \\ & \quad - \frac{7}{216} \left[ k_1^{n_V-2} k_2^{n_V-6} + 5 \text{ perms.} \right] \\ & \quad + \frac{5}{216} \left[ k_1^{n_V-6} k_2^{n_V-4} k_3^2 + 5 \text{ perms.} \right] \\ & \quad + \frac{1}{72} \left[ k_1^{-2} k_2^{n_V} k_3^{n_V-6} + 5 \text{ perms.} \right] \\ & \quad - \frac{1}{72} \left[ k_1^{-2} k_2^{n_V-2} k_3^{n_V-4} + 5 \text{ perms.} \right] \\ & \quad - \frac{1}{216} \left[ k_1^{n_V-6} k_2^{n_V-6} k_3^4 + 2 \text{ perms.} \right]. \end{aligned} \quad (10)$$

This overall shape is illustrated in Fig. 1. We can see that the bispectrum for  $n_V \sim 1$  is enhanced in the squeezed limit ( $k_3 \ll k_1 \approx k_2$ ) and close to the local-type configuration. This may be due to a fact that anisotropic stress  $\Pi_{Vj}^i$  is localized in real space like the local-type non-Gaussianity. The local-type curvature perturbation is written as  $\mathcal{R}_{\text{loc}}(\mathbf{x}) =$

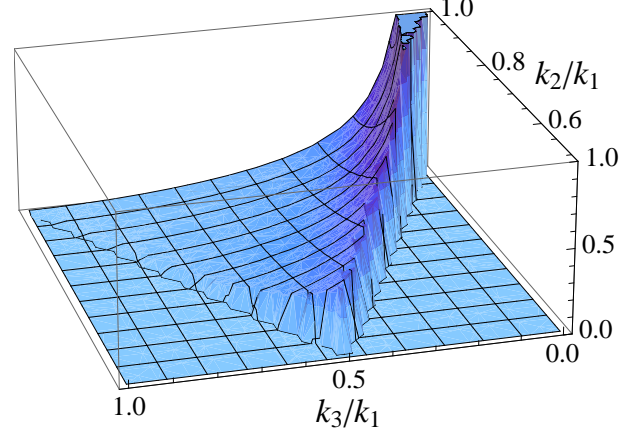


**Figure 1.** Shape of  $k_1^2 k_2^2 k_3^2 S_V(n_V = 1)$ . Due to the symmetric property and triangle inequality, the plot range is restricted as  $k_3 \leq k_2 \leq k_1$  and  $|k_1 - k_2| \leq k_3 \leq k_1 + k_2$ . It is shown that the bispectrum diverges in the squeezed limit as  $k_3 \ll k_1 \approx k_2$ .

$\mathcal{R}_g(\mathbf{x}) + \frac{3}{5} f_{\text{NL}} [\mathcal{R}_g^2(\mathbf{x}) - \langle \mathcal{R}_g^2(\mathbf{x}) \rangle]$  with  $f_{\text{NL}}$  and  $\mathcal{R}_g$  denoting the local-type nonlinear parameter and the Gaussian perturbation, respectively (e.g., Komatsu & Spergel (2001)). Then, the local-type bispectrum is given by

$$\left\langle \prod_{n=1}^3 \mathcal{R}_{\text{loc}}(\mathbf{k}_n) \right\rangle \equiv (2\pi)^3 B_{\mathcal{R}_{\text{loc}}}(k_1, k_2, k_3) \delta\left(\sum_{n=1}^3 \mathbf{k}_n\right), \quad (11)$$

with

$$\begin{aligned} B_{\mathcal{R}_{\text{loc}}} &= \frac{6}{5} f_{\text{NL}} [P_{\mathcal{R}_g}(k_1) P_{\mathcal{R}_g}(k_2) + 2 \text{ perms.}] \\ &= \frac{3}{5} f_{\text{NL}} (2\pi^2 A_{\text{loc}})^2 k_*^{2(1-n_{\text{loc}})} S_{\text{loc}}(k_1, k_2, k_3), \end{aligned} \quad (12)$$

$$S_{\text{loc}} \equiv 2k_1^{n_{\text{loc}}-4} k_2^{n_{\text{loc}}-4} + 2 \text{ perms.} . \quad (13)$$

Here,  $P_{\mathcal{R}_g} \equiv \frac{2\pi^2}{k^3} A_{\text{loc}} \left(\frac{k}{k_*}\right)^{n_{\text{loc}}-1}$  is the power spectrum of  $\mathcal{R}_g$ ,  $n_{\text{loc}}$  is the spectral index, and  $A_{\text{loc}} = 2.43 \times 10^{-9}$  is a normalization factor obtained from the observational data of the scalar power spectrum (Komatsu et al. (2011)). The correlation coefficient between  $S_V$  and  $S_{\text{loc}}$  is about 0.96 for  $n_V = n_{\text{loc}} \sim 1$ , which quantitatively shows the consistency with the local-type bispectrum. Actually, we can see that in the squeezed limit ( $k \ll k'$ ), these shape functions have the same  $k$  dependence as

$$S_V(k, k', k') \approx \frac{2}{27} k^{n_V-4} k'^{n_V-4}, \quad (14)$$

$$S_{\text{loc}}(k, k', k') \approx 4k^{n_{\text{loc}}-4} k'^{n_{\text{loc}}-4}. \quad (15)$$

By using an approximate proportional relation:  $S_V \approx 0.0238 S_{\text{loc}}$ , which is derived by numerical evaluation, we can construct an approximate relation as

$$\begin{aligned} F_V^3 &= \frac{4}{15} \frac{n_V - 1}{\beta_{n_V}} \frac{S_{\text{loc}}}{S_V} f_{\text{NL}} A_{\text{loc}}^2 \\ &\approx f_{\text{NL}} \times \begin{cases} 8.43 \times 10^{-18} & (n_V = 1.1) \\ 6.39 \times 10^{-19} & (n_V = 1.01) \end{cases}. \end{aligned} \quad (16)$$

In the next section, we will check whether or not this relation is valid even in the scale-dependent bias.

<sup>2</sup> The relation between  $\beta_{1.1}$  and  $\alpha (= 0.335)$  of Shiraishi et al. (2012) is given by

$$\beta_{1.1} = \left( \frac{10 \text{Mpc}^{-1}}{k_*} \right)^{0.1} \alpha.$$

### 2.3 Interpretation as the electromagnetic field

Such non-Gaussian anisotropic stress can be created in the framework of the inflationary models involving a conformally variant coupling between the scalar field  $\phi$  and the vector field  $A_\mu$ , whose action is expressed as  $S \supset - \int d^4x \frac{1}{4} \sqrt{-g} g^{\mu\lambda} g^{\nu\sigma} W(\phi) F_{\mu\nu} F_{\lambda\sigma}$  (e.g., Caldwell et al. (2011); Motta & Caldwell (2012); Barnaby et al. (2012)). Here,  $F_{\mu\nu} \equiv \partial_\mu A_\nu - \partial_\nu A_\mu$ , and  $W(\phi)$  denotes the running coupling which induces the violation of the conformal invariance. Then, on a natural assumption that the inflaton falls into a stable state,  $W(\phi)$  freezes out at the end of inflation as  $W(\phi) \rightarrow W_I$ , and the conformal invariance restores, we may have residual anisotropic stress generated from the electromagnetic field ( $\mathbf{E}$  and  $\mathbf{B}$ ) at later times. According to Shiraishi et al. (2012), if we take  $f_V = -W_I$ ,  $V_i$  in equation (3) can be then equated to  $E_i/\sqrt{4\pi\rho_{\gamma,0}}$  or  $B_i/\sqrt{4\pi\rho_{\gamma,0}}$ .

From here, let us focus on a case that the electric field disappears due to the Coulomb screening in the primordial plasma and only the magnetic field survives at late times with  $W_I = 1$ . This setting has been often considered in the context of the cosmological magnetogenesis while there remain outstanding issues such as the so-called strong coupling or backreaction problem (e.g., Demozzi et al. (2009); Barnaby et al. (2012); Fujita & Mukohyama (2012)). In such a case, a conventional parametrization of the magnetic field is given as (Shaw & Lewis (2010); Shiraishi et al. (2012))

$$\langle B^i(\mathbf{k}) B_j(\mathbf{k}') \rangle = (2\pi)^3 \frac{P_B(k)}{2} P_j^i(\hat{\mathbf{k}}) \delta(\mathbf{k} + \mathbf{k}'), \quad (17)$$

$$P_B(k) \equiv A_B k^{n_B}, \quad (18)$$

$$A_B = \frac{(2\pi)^{n_B+5} B_r^2}{\Gamma\left(\frac{n_B+3}{2}\right) k_r^{n_B+3}} \quad (n_B > -3), \quad (19)$$

where  $B_r$  denotes the magnetic field strength smoothed on the scale  $r$ ,  $k_r \equiv 2\pi/r$ ,  $n_B$  is the spectral index of the magnetic power spectrum, and  $\Gamma(x)$  is the Gamma function. Diverse analyses of the cosmological phenomena such as the CMB anisotropy and the large scale structure suggest constraints on these parameters as  $B_{1\text{Mpc}} < \mathcal{O}(0.1 - 1)\text{nG}$  and  $n_B \sim -3$  (e.g., Shaw & Lewis (2012); Paoletti & Finelli (2011); Shiraishi et al. (2012); Yamazaki et al. (2012); Pandey & Sethi (2013); Paoletti & Finelli (2012)). Accordingly, we hold the correspondence:

$$A_V = \frac{A_B k_*^{n_V-1}}{8\pi^3 \rho_{\gamma,0}}, \quad (20)$$

$$n_V = n_B + 4. \quad (21)$$

Interestingly, for the magnetic case, because of  $f_V = -1$  and  $B_{1\text{Mpc}} \geq 0$ , the resultant bispectrum of curvature perturbations can mimic the local-type bispectrum with only  $f_{\text{NL}} \leq 0$ . Owing to this, an approximate relation for the vector field (16) is translated into

$$\begin{aligned} & \left( \frac{B_{1\text{Mpc}}}{\text{lnG}} \right) \left( \frac{\ln(\tau_\nu/\tau_B)}{\ln 10^{17}} \right)^{1/2} \\ & \approx (-f_{\text{NL}})^{1/6} \times \begin{cases} 2.92 & (n_B = -2.9) \\ 4.60 & (n_B = -2.99) \end{cases}. \end{aligned} \quad (22)$$

This analytic evaluation implies that the bispectrum from the magnetic field and the local-type bispectrum with neg-

ative  $f_{\text{NL}}$  give similar impacts also on the scale-dependent bias parameters as shown in the following section.

## 3 SCALE-DEPENDENT BIAS ORIGINATED FROM VECTOR FIELD

Recently, in Matsubara (2012), by applying the integrated perturbation theory (IPT) (Matsubara (2011)), more general formalism for the scale-dependent bias have been constructed. In this section, employing this formalism, we estimate the bias parameter from non-Gaussian anisotropic stress driven by the vector field.

### 3.1 Formulation

The bias parameters are often defined in the relation between the biased power spectrum of objects  $X$ ,  $P_X$ , and the linear matter power spectrum,  $P_L$ :

$$P_X(k) \equiv [b + \Delta b(k, M)]^2 P_L(k), \quad (23)$$

where  $b$  denotes the scale-independent Eulerian linear bias parameter and  $\Delta b$  is the scale-dependent bias parameter arising from the primordial non-Gaussianity. In the literature, we also see another notation of the bias parameters, which links the cross-correlation between the linearized matter density field and objects  $X$ ,  $P_{LX}$ , to  $P_L$  as

$$P_{LX}(k) \equiv [b + \Delta b(k, M)] P_L(k). \quad (24)$$

These two  $\Delta b$ 's are identical under the situation that the non-Gaussianity is so weak that the contribution of the trispectrum can be negligible (Matsubara (2012)). In other words, considering a highly non-Gaussian source,  $\Delta b$  in equation (23) is affected by the higher-order correlations and may differ from  $\Delta b$  in equation (24) at large scales (Yokoyama (2011); Yokoyama & Matsubara (2012)). Here, we shall blink this fact tentatively and formulate the scale-dependent bias arising from the bispectrum of curvature perturbations.

According to Matsubara (2012), the scale-dependent bias parameter is expressed as

$$\Delta b(k, M) \approx \frac{\sigma_M^2}{2\delta_c^2} \left[ A_2(M) \mathcal{I}(k, M) + A_1(M) \frac{\partial \mathcal{I}(k, M)}{\partial \ln \sigma_M} \right], \quad (25)$$

where  $\delta_c = 1.686$  is the critical overdensity and

$$\begin{aligned} \mathcal{I}(k, M) &= \frac{1}{\sigma_M^2 P_L(k)} \int \frac{d^3 \mathbf{k}'}{(2\pi)^3} W(k'R) W(|\mathbf{k} - \mathbf{k}'|R) \\ &\quad \times B_L(k, k', |\mathbf{k} - \mathbf{k}'|). \end{aligned} \quad (26)$$

The coefficients  $A_1$  and  $A_2$  are expanded by the Lagrangian bias parameters  $b_1^L$  and  $b_2^L$  as

$$A_1(M) = 1 + \delta_c b_1^L(M), \quad (27)$$

$$A_2(M) = 2 + 2\delta_c b_1^L(M) + \delta_c^2 b_2^L(M). \quad (28)$$

Following the notation of the halo model, we have introduced the Lagrangian radius  $R$  satisfying  $M = \frac{4\pi}{3} \Omega_{m0} \rho_{c0} R^3$ , which is equivalent to

$$\frac{R}{\text{Mpc}} = \left[ \frac{M}{1.162 \times 10^{12} h^2 M_\odot \Omega_{m0}} \right]^{1/3}. \quad (29)$$

Here,  $\rho_{c0}$  and  $\Omega_{m0}$  are the present values of the critical density and the matter density parameter, respectively,  $h \equiv H_0/(100\text{km/sec/Mpc})$  with  $H_0$  being the Hubble constant, and  $M_\odot = 1.989 \times 10^{30}\text{kg}$  is the mass of the sun. Then, the density variance is defined by

$$\sigma_M^2 = \int \frac{k^2 dk}{2\pi^2} W^2(kR) P_L(k), \quad (30)$$

where we choose a top-hat window function as

$$W(x) = \frac{3j_1(x)}{x}, \quad (31)$$

with  $j_\ell(x)$  being the spherical Bessel function.

The Lagrangian bias parameters,  $b_1^L$  and  $b_2^L$ , depend on the shape of the mass function. In our numerical calculation, we adapt the fitting formulae derived from ‘‘MICE mass function’’, which has been estimated from the data of MICE simulations (Croce et al. (2010)), as

$$b_1^L(M) = \frac{1}{\delta_c} \left( \frac{2c_3}{\sigma_M^2} - \frac{c_1}{1 + c_2\sigma_M^{c_1}} \right), \quad (32)$$

$$b_2^L(M) = \frac{1}{\delta_c^2} \left[ \frac{4c_3^2}{\sigma_M^4} - \frac{2c_3}{\sigma_M^2} - \frac{c_1(4c_3/\sigma_M^2 - c_1 + 1)}{1 + c_2\sigma_M^{c_1}} \right], \quad (33)$$

with  $c_1 = 1.37a^{0.15}$ ,  $c_2 = 0.3a^{0.084}$  and  $c_3 = 1.036a^{0.024}$ .

The linear matter power spectrum,  $P_L$ , and the bispectrum sourced from the primordial non-Gaussianity,  $B_L$ , are expressed as

$$P_L(k) = \mathcal{M}_{\mathcal{R}}^2(k) P_{\mathcal{R}}(k), \quad (34)$$

$$B_L(k_1, k_2, k_3) = \left[ \prod_{n=1}^3 \mathcal{M}_{\mathcal{R}}(k_n) \right] B_{\mathcal{R}}(k_1, k_2, k_3), \quad (35)$$

where  $\mathcal{M}_{\mathcal{R}}$  denotes the conversion function involving the information of the linear evolution of the matter contrast and is parametrized as

$$\mathcal{M}_{\mathcal{R}}(k) = \frac{2}{5} D(a) \frac{k^2 T(k)}{H_0^2 \Omega_{m0}}. \quad (36)$$

The matter transfer function  $T(k)$  and the growth factor  $D(a)$  are realized by such fitting functions as (Lahav et al. (1991); Weinberg (2008))

$$T(k) = \frac{\ln[1 + (0.124\kappa)^2]}{(0.124\kappa)^2} \times \sqrt{\frac{1 + (1.257\kappa)^2 + (0.4452\kappa)^4 + (0.2197\kappa)^6}{1 + (1.606\kappa)^2 + (0.8568\kappa)^4 + (0.3927\kappa)^6}}, \quad (37)$$

with

$$\kappa = \frac{k\sqrt{\Omega_{r0}}}{H_0\Omega_{m0}} \left[ \alpha + \frac{1 - \alpha}{1 + (0.43ks)^4} \right]^{-1}, \quad (38)$$

$$\alpha = 1 - 0.328 \ln(431\Omega_{m0}h^2) \frac{\Omega_{b0}}{\Omega_{m0}} + 0.38 \ln(22.3\Omega_{m0}h^2) \left( \frac{\Omega_{b0}}{\Omega_{m0}} \right)^2, \quad (39)$$

$$s = \frac{44.5 \ln[9.83/(\Omega_{m0}h^2)]}{\sqrt{1 + 10(\Omega_{b0}h^2)^{3/4}}} \text{Mpc}, \quad (40)$$

and

$$D(a) = \frac{5}{2} a \Omega_m \times \left[ \Omega_m^{4/7} - \Omega_\Lambda + \left( 1 + \frac{\Omega_m}{2} \right) \left( 1 + \frac{\Omega_\Lambda}{70} \right) \right]^{-1}. \quad (41)$$

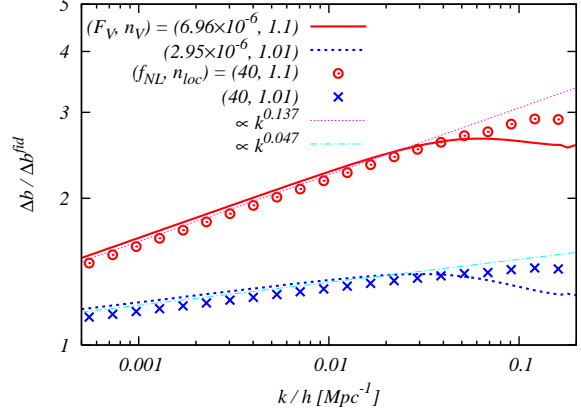


**Figure 2.** Scale-dependent bias parameters normalized by  $\Delta b^{\text{loc}}$  for  $(f_{\text{NL}}, n_{\text{loc}}) = (40, 0.963)$  (corresponding to  $\Delta b^{\text{fid}}$ ) at redshift  $z \equiv a^{-1} - 1 = 1$ . Red solid and blue dotted lines correspond to  $\Delta b^V / \Delta b^{\text{fid}}$ , and red circles and blue crosses denote  $\Delta b^{\text{loc}} / \Delta b^{\text{fid}}$  with  $f_{\text{NL}} = 40$ , respectively, when  $n_V = n_{\text{loc}} = 1.1, 1.01$ . The parameters of these amplitudes are taken to satisfy the approximate relation (16) as seen in the graph legends. The other related parameters are fixed as  $\Omega_{m0} = 0.275$ ,  $\Omega_{\Lambda 0} = 1 - \Omega_{m0}$ ,  $h = 0.7$  and  $M/M_\odot = 10^{14}$ . Magenta fine dotted and cyan chain lines with the  $k$  dependence as the graph legends are plotted for the check of the scaling relations (46).

Here,  $\Omega_{\Lambda 0}, \Omega_{b0}$  and  $\Omega_{r0}$  are the present density parameter of the cosmological constant, baryon and radiation, respectively,  $\Omega_m(a) \equiv \frac{\Omega_{m0}}{\Omega_{m0} + a^3 \Omega_{\Lambda 0}}$ , and  $\Omega_\Lambda(a) \equiv \frac{a^3 \Omega_{\Lambda 0}}{\Omega_{m0} + a^3 \Omega_{\Lambda 0}}$ . In the matter dominated era,  $D(a)$  converges to  $a$ .

To obtain the scale-dependent biases from the primordial vector field and the local-type non-Gaussianity, we only input several power spectra and bispectra described in the previous section to equation (25).

### 3.2 Analysis

Let us focus on the numerical analysis of the scale-dependent bias from the vector field,  $\Delta b^V$ . For comparison, we also calculate the scale-dependent bias from the local-type bispectrum,  $\Delta b^{\text{loc}}$ . In what follows, as the value of the power spectrum of curvature perturbations, we adopt an observational consequence by the WMAP experiment as (Komatsu et al. (2011))

$$P_{\mathcal{R}}(k) \equiv \frac{2\pi^2}{k^3} A_{\mathcal{R}} \left( \frac{k}{k_*} \right)^{n_{\mathcal{R}} - 1}, \quad (42)$$

with  $A_{\mathcal{R}} = A_{\text{loc}} = 2.43 \times 10^{-9}$  and  $n_{\mathcal{R}} = 0.963$ . In our case, the vector field creates not only the bispectrum but also the power spectrum of curvature perturbations, namely,  $P_{\mathcal{R}_V}$ , as calculated in Appendix A. In this sense,  $P_{\mathcal{R}_V}$  becomes part of  $P_{\mathcal{R}}$  along with the power spectra from other sources such as the cross-bispectra between metric perturbations and electromagnetic fields (e.g., Shiraishi et al. (2012); Kunze (2012)). By lack of the explicit dependence of  $P_{\mathcal{R}}$  on  $F_V$ ,  $\Delta b^V$  is simply proportional to  $F_V^3$ .

In Fig. 2, we plot the ratios of  $\Delta b^V$  and  $\Delta b^{\text{loc}}$  to  $\Delta b^{\text{fid}} \equiv \Delta b^{\text{loc}}(f_{\text{NL}} = 40, n_{\text{loc}} = n_{\mathcal{R}})$  for the parameters satisfying the approximate relation (16) when  $f_{\text{NL}} = 40$  and  $n_V = n_{\text{loc}} = 1.1, 1.01$ . From this figure, it is observed

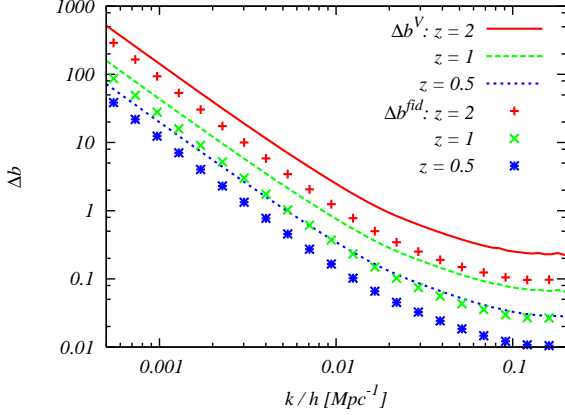


**Figure 3.** Scale-dependent bias parameters for  $z = 2, 1, 0.5$ . Each kind of line and point corresponds to  $\Delta b^V$  with  $(F_V, n_V) = (6.96 \times 10^{-6}, 1.1)$  and  $\Delta b^{\text{fid}}$ , respectively (see the graph legends). The related parameters are identical to the values represented in Fig. 2.

that the red solid (blue dotted) line is in agreement with red circles (blue crosses) at large scales. This fact indicates that the approximate relation (16) is true even in the scale-dependent bias. On the other hand, the deviation at small scales may be due to the tiny difference of  $k$  dependence between the primordial bispectra (10) and (13). This may become key signals in order to extract the information of the vector field from the contamination of other local-type non-Gaussian sources.

If one see red solid and blue dotted curves of this figure, one can notice that the difference of tilt between  $\Delta b^V$  ( $n_V = 1.1$ ) and  $\Delta b^V$  ( $n_V = 1.01$ ) is evident. This different  $k$  dependence can be analytically estimated as follows. Picking up the  $k$ -dependent part in equation (25), we have

$$\Delta b(k) \propto \frac{1}{P_L(k)} \int \frac{d^3 \mathbf{k}'}{(2\pi)^3} W(k'R) W(|\mathbf{k} - \mathbf{k}'|R) \times B_L(k, k', |\mathbf{k} - \mathbf{k}'|). \quad (43)$$

In the large-scale limit, the integrand of this equation reduces to the form under the squeezed limit ( $k \ll k'$ ), i.e.,

$$W(|\mathbf{k} - \mathbf{k}'|R) \approx W(k'R), \quad (44)$$

$$B_L(k, k', |\mathbf{k} - \mathbf{k}'|) \approx \mathcal{M}_{\mathcal{R}}(k) \mathcal{M}_{\mathcal{R}}^2(k') B_{\mathcal{R}}(k, k', k'). \quad (45)$$

Using the squeezed-limit forms of the shape functions (14) and (15), the large-scale approximation of the matter transfer function as  $T(k) \approx 1$ , namely,  $\mathcal{M}_{\mathcal{R}}(k) \propto k^2$ , and  $P_{\mathcal{R}}(k) \propto k^{n_{\mathcal{R}}-4}$ , we obtain the scaling relation of each bias at large scales as

$$\begin{aligned} \Delta b^V(k) &\propto k^{n_V - n_{\mathcal{R}} - 2} \\ \Delta b^{\text{loc}}(k) &\propto k^{n_{\text{loc}} - n_{\mathcal{R}} - 2}, \\ \Delta b^{\text{fid}}(k) &\propto k^{-2}. \end{aligned} \quad (46)$$

The  $k$  dependences derived from these equations,  $\Delta b / \Delta b^{\text{fid}} \propto k^{0.137}$  for  $n_V = n_{\text{loc}} = 1.1$  and  $k^{0.047}$  for  $n_V = n_{\text{loc}} = 1.01$ , fit well to the curves and points of Fig. 2.

Figure 3 shows the redshift dependence of  $\Delta b^V$  and  $\Delta b^{\text{fid}}$ . We can see that as  $z$  evolves, the overall amplitudes of  $\Delta b^V$  and  $\Delta b^{\text{fid}}$  simply decreases while their shapes are kept, respectively. Such multi- $z$  information will become

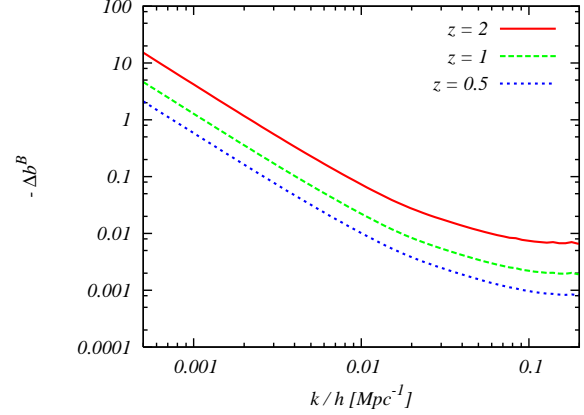


**Figure 4.** Scale-dependent bias parameter from the primordial magnetic field for  $z = 2, 1, 0.5$  (describe  $-\Delta b^B$ ). Here, the parameters of the magnetic field are taken to be consistent with observations as  $(B_{1\text{Mpc}}, \tau_\nu / \tau_B, n_B) = (3\text{nG}, 10^{17}, -2.9)$ . The other parameters are identical to the values represented in Fig. 2.

more valuable when we analyze the tomographic data from BOSS and forthcoming EUCLID experiments (Ross et al. (2012); Laureijs et al. (2011)).

In the remaining part, we examine how the magnetic field affects the scale-dependent bias. As shown in Section. 2.3, the bispectrum of curvature perturbations induced by magnetic anisotropic stresses corresponds to the bispectrum with only negative  $f_{\text{NL}}$ . This dependence appears also in the scale-dependent bias. Figure 4 describes the scale-dependent bias from the magnetic field,  $\Delta b^B$ , for each redshift. We here choose the magnetic parameters:  $(B_{1\text{Mpc}}, \tau_\nu / \tau_B, n_B) = (3\text{nG}, 10^{17}, -2.9)$ , which are consistent with the current observational bounds (e.g., Shaw & Lewis (2012); Paoletti & Finelli (2011); Shiraishi et al. (2012); Yamazaki et al. (2012); Paoletti & Finelli (2012); Pandey & Sethi (2013)). In this case,  $\Delta b^B$  is equivalent to  $\Delta b^V$  for  $(F_V, n_V) = (-2.15 \times 10^{-6}, 1.1)$ . Translating this magnetic field into the local-type non-Gaussianity for  $n_{\text{loc}} = 1.1$  by use of equation (22), we have  $f_{\text{NL}} = -1.2$ . From this figure, one can confirm that  $\Delta b^B$  has negative values at all  $k$ . This negative impact with the deviation from the fiducial  $k$  dependence as  $\Delta b^{\text{fid}} \propto k^{-2}$  can change more or less entire shape of the scale-dependent bias parameter and become a key feature to probe the primordial magnetic field.

### 3.3 On higher-order effect

In the above evaluation, we took into account the effects of only the bispectrum of curvature perturbations. However, there remain a concern about the contribution of the higher-order correlation because curvature perturbation driven by the vector field (1) is the Gaussian-squared field, i.e., highly non-Gaussian field. In Yokoyama (2011), the halo-halo bias has been computed when the curvature perturbation is sourced from the Gaussian-squared scalar field. For this case, we have a consistency relation between the nonlinearity parameters associated with the bispectrum and trispectrum of curvature perturbations as  $\tau_{\text{NL}} \sim 500 f_{\text{NL}}^{4/3}$ . If the angular dependence due to the vector field is negligible, this relation

may be applicable to our case. Then, considerable trispectrum contribution may modify the halo-halo bias from the vector field at large scales as pointed out in Yokoyama (2011); Yokoyama & Matsubara (2012). However, this effect is sensitive to a coefficient of  $f_{\text{NL}}^{4/3}$  in the above relation and hence detailed calculation with the complicated angular dependence is required for precise discussion. It remains as a future issue.

#### 4 SUMMARY AND DISCUSSION

This paper investigates the scale-dependent bias, which arises from the non-Gaussianity of curvature perturbations due to anisotropic stress induced by the Gaussian vector field. This non-Gaussianity induces the local-type bispectrum of curvature perturbations. We found an approximate relation between the strength of anisotropic stress from the vector field  $F_V$  and the local-type nonlinearity parameter  $f_{\text{NL}}$  as shown in equation (16). Via numerical calculation, we demonstrated that as this relation predicts, the scale-dependent bias from the vector field is in agreement with that from the local-type non-Gaussianity at large scales. At the same time, we also observed the deviation from the local-type bias at small scales. This feature may be useful for seeking the evidence of the primordial vector field from the observational result of the scale-dependent bias. Furthermore, the  $k$  dependence of the scale-dependent bias directly reflects the spectral tilt of the power spectrum of vector fields as shown in equation (46). In this sense, via the observational consequence for the  $k$  dependence, we will also approach the shape of the primordial vector field. By interpreting the primordial vector field as the primordial magnetic field, we reached a fact that the scale-dependent bias has negative values. This is an interesting consequence and helpful to constrain the primordial magnetic field. Comparing the theoretical results involving the contribution of the higher-order correlations with the observational data leads to further understanding of the nature of the vector field.

#### ACKNOWLEDGMENTS

This work was supported in part by a Grant-in-Aid for JSPS Research under Grant Nos. 22-7477 (MS) and 24-2775 (SY), a Grant-in-Aid for Scientific Research under Grant Nos. 24340048 (KI) and 24540267 (TM), and Grant-in-Aid for Nagoya University Global COE Program “Quest for Fundamental Principles in the Universe: from Particles to the Solar System and the Cosmos”, from the Ministry of Education, Culture, Sports, Science and Technology of Japan. We also acknowledge the Kobayashi-Maskawa Institute for the Origin of Particles and the Universe, Nagoya University, for providing computing resources useful in conducting the research reported in this paper.

#### REFERENCES

- Ackerman L., Carroll S. M., Wise M. B., 2007, *Phys. Rev.*, D75, 083502, astro-ph/0701357  
 Bamba K., Sasaki M., 2007, *JCAP*, 0702, 030, astro-ph/0611701  
 Bamba K., Yokoyama J., 2004, *Phys.Rev.*, D69, 043507, astro-ph/0310824  
 Barnaby N., Moxon J., Namba R., Peloso M., Shiu G., et al., 2012, *Phys.Rev.*, D86, 103508, 1206.6117  
 Barnaby N., Namba R., Peloso M., 2011, *JCAP*, 1104, 009, 1102.4333  
 Barnaby N., Namba R., Peloso M., 2012, *Phys.Rev.*, D85, 123523, 1202.1469  
 Barnaby N., Peloso M., 2011, *Phys.Rev.Lett.*, 106, 181301, 1011.1500  
 Bartolo N., Komatsu E., Matarrese S., Riotto A., 2004, *Phys. Rept.*, 402, 103, astro-ph/0406398  
 Bartolo N., Matarrese S., Peloso M., Ricciardone A., 2012, 1210.3257  
 Becker A., Huterer D., 2012, *Phys.Rev.Lett.*, 109, 121302, 1207.5788  
 Becker A., Huterer D., Kadota K., 2012, 1206.6165  
 Brown I., Crittenden R., 2005, *Phys. Rev.*, D72, 063002, astro-ph/0506570  
 Caldwell R. R., Motta L., Kamionkowski M., 2011, *Phys.Rev.*, D84, 123525, 1109.4415  
 Crocce M., Fosalba P., Castander F. J., Gaztanaga E., 2010, *Mon.Not.Roy.Astron.Soc.*, 403, 1353, 0907.0019  
 Demozzi V., Mukhanov V., Rubinstein H., 2009, *JCAP*, 0908, 025, 0907.1030  
 Demozzi V., Ringeval C., 2012, *JCAP*, 1205, 009, 1202.3022  
 Dimastrogiovanni E., Bartolo N., Matarrese S., Riotto A., 2010, *Adv.Astron.*, 2010, 752670, 1001.4049  
 Fujita T., Mukohyama S., 2012, *JCAP*, 1210, 034, 1205.5031  
 Hikage C., Matsubara T., 2012, *Mon.Not.Roy.Astron.Soc.*, 425, 2187, 1207.1183  
 Jain R. K., Sloth M. S., 2012, *Phys.Rev.*, D86, 123528, 1207.4187  
 Kanno S., Soda J., Watanabe M.-a., 2009, *JCAP*, 0912, 009, 0908.3509  
 Karciuskas M., Dimopoulos K., Lyth D. H., 2009, *Phys.Rev.*, D80, 023509, 0812.0264  
 Kojima K., Kajino T., Mathews G. J., 2010, *JCAP*, 1002, 018, 0910.1976  
 Komatsu E., 2010, *Class. Quant. Grav.*, 27, 124010, 1003.6097  
 Komatsu E., et al., 2011, *ApJS*, 192, 18, 1001.4538  
 Komatsu E., Spergel D. N., 2001, *Phys. Rev.*, D63, 063002, astro-ph/0005036  
 Kunze K. E., 2012, 1209.4570  
 Lahav O., Lilje P. B., Primack J. R., Rees M. J., 1991, *Mon.Not.Roy.Astron.Soc.*, 251, 128  
 Laureijs R., Amiaux J., Arduini S., Augueres J.-L., Brinchmann J., et al., 2011, 1110.3193  
 Martin J., Yokoyama J., 2008, *JCAP*, 0801, 025, 0711.4307  
 Matsubara T., 2011, *Phys.Rev.*, D83, 083518, 1102.4619  
 Matsubara T., 2012, *Phys.Rev.*, D86, 063518, 1206.0562  
 Motta L., Caldwell R. R., 2012, *Phys.Rev.*, D85, 103532, 1203.1033  
 Pandey K. L., Sethi S. K., 2013, *Astrophys.J.*, 762, 15, 1210.3298  
 Paoletti D., Finelli F., 2011, *Phys.Rev.*, D83, 123533, 1005.0148  
 Paoletti D., Finelli F., 2012, 1208.2625  
 Ross A. J., Percival W. J., Carnero A., Zhao G.-b., Manera M., et al., 2012, 1208.1491

- Sefusatti E., Liguori M., Yadav A. P., Jackson M. G., Pajer E., 2009, JCAP, 0912, 022, 0906.0232
- Shandera S., Dalal N., Huterer D., 2011, JCAP, 1103, 017, 1010.3722
- Shaw J. R., Lewis A., 2010, Phys.Rev., D81, 043517, 0911.2714
- Shaw J. R., Lewis A., 2012, Phys.Rev., D86, 043510, 1006.4242
- Shiraishi M., 2012, JCAP, 1206, 015, 1202.2847
- Shiraishi M., Nitta D., Yokoyama S., Ichiki K., 2012, JCAP, 1203, 041, 1201.0376
- Shiraishi M., Saga S., Yokoyama S., 2012, JCAP, 1211, 046, 1209.3384
- Slosar A., Hirata C., Seljak U., Ho S., Padmanabhan N., 2008, JCAP, 0808, 031, 0805.3580
- Smidt J., Amblard A., Byrnes C. T., Cooray A., Heavens A., et al., 2010, Phys.Rev., D81, 123007, 1004.1409
- Sorbo L., 2011, JCAP, 1106, 003, 1101.1525
- Suyama T., Yokoyama J., 2012, Phys.Rev., D86, 023512, 1204.3976
- Valenzuela-Toledo C. A., Rodriguez Y., 2010, Phys.Lett., B685, 120, 0910.4208
- Verde L., 2010, Adv.Astron., 2010, 768675, 1001.5217
- Watanabe M.-a., Kanno S., Soda J., 2010, Prog.Theor.Phys., 123, 1041, 1003.0056
- Watanabe M.-a., Kanno S., Soda J., 2011, Mon.Not.Roy.Astron.Soc., 412, L83, 1011.3604
- Weinberg S., 2008, Cosmology. Oxford University Press, ADS
- Widrow L. M., 2002, Rev. Mod. Phys., 74, 775, astro-ph/0207240
- Yamazaki D. G., Kajino T., Mathew G. J., Ichiki K., 2012, Phys.Rept., 517, 141, 1204.3669
- Yokoyama S., 2011, JCAP, 1111, 001, 1108.5569
- Yokoyama S., Matsubara T., 2012, 1210.2495
- Yokoyama S., Soda J., 2008, JCAP, 0808, 005, 0805.4265

## APPENDIX A: POWER SPECTRUM OF CURVATURE PERTURBATIONS INDUCED FROM VECTOR FIELD

Here, we present the analytic formula for the power spectrum of curvature perturbations arising from anisotropic stress composed of the square of the Gaussian vector field. From equations in Section 2, this is formed as

$$\left\langle \prod_{n=1}^2 \mathcal{R}_V(\mathbf{k}_n) \right\rangle = (2\pi)^3 P_{\mathcal{R}_V}(k_1) \delta\left(\sum_{n=1}^2 \mathbf{k}_n\right), \quad (\text{A1})$$

$$P_{\mathcal{R}_V}(k) = \frac{2\pi^2}{k^3} F_V^2 \frac{\pi_{n_V}}{4} \left(\frac{k}{k_*}\right)^{2(n_V-1)}. \quad (\text{A2})$$

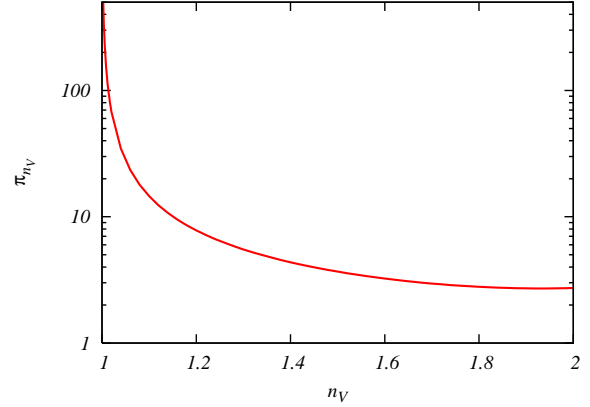


**Figure A1.** Dependence of  $\pi_{n_V}$  on  $n_V$ .

A factor  $\pi_{n_V}$  arises from the convolution in terms of  $P_V(k)$  as

$$\begin{aligned} \pi_{n_V} &= \frac{k^{-2n_V+5}}{2\pi} \int d^3\mathbf{k}' k'^{n_V-4} |\mathbf{k} - \mathbf{k}'|^{n_V-4} \\ &\times \left[ 1 - \frac{3}{4}(\beta^2 + \gamma^2) + \frac{9}{4}\beta^2\gamma^2 - \frac{3}{2}\mu\gamma\beta + \frac{1}{4}\mu^2 \right] \\ &= \int_0^\infty du u^{n_V-2} \int_{-1}^1 d\gamma (1 - 2u\gamma + u^2)^{(n_V-4)/2} \\ &\times \left[ 1 - \frac{3}{4}(\beta^2 + \gamma^2) + \frac{9}{4}\beta^2\gamma^2 - \frac{3}{2}\mu\gamma\beta + \frac{1}{4}\mu^2 \right], \end{aligned} \quad (\text{A3})$$

where the parameters are corresponding to

$$u = \frac{k'}{k}, \quad (\text{A4})$$

$$\gamma = \hat{\mathbf{k}} \cdot \hat{\mathbf{k}}', \quad (\text{A5})$$

$$\mu = \hat{\mathbf{k}}' \cdot \widehat{\mathbf{k} - \mathbf{k}'} = \frac{\gamma - u}{\sqrt{1 + u^2 - 2u\gamma}}, \quad (\text{A6})$$

$$\beta = \hat{\mathbf{k}} \cdot \widehat{\mathbf{k} - \mathbf{k}'} = \frac{1 - u\gamma}{\sqrt{1 + u^2 - 2u\gamma}}, \quad (\text{A7})$$

$$|\mathbf{k} - \mathbf{k}'|^2 = k^2 (1 + u^2 - 2u\gamma). \quad (\text{A8})$$

While the integral over  $\gamma$  can be analytically evaluated, we have to rely on numerical calculation in the integral over  $k$ . In Fig. A1, we show  $\pi_{n_V}$  for  $1 < n_V < 2$ . It can be seen that as  $n_V$  decreases, the contribution around a pole dominates and  $\pi_{n_V}$  is boosted.